Spatial and temporal patterns of forest disturbance and regrowth in PT Singlurus Pratama coal mine reclamation area, East Kalimantan, Indonesia

1. Introduction

The Earth's surface has changed dramatically over the past several centuries. The primary force behind this change has been land-use, and perhaps no land-use practices affected the biosphere more than open-pit mining (Cohen et all, 2010). This is especially a severe issue in the tropical areas in the XXI century because of forests' role in decreasing greenhouse gases. Thus, there is a need for long-term monitoring of open-pit mine sites to provide scientific data for ongoing ecological management after extraction of the mineral resources is over (Zhu et all, 2019).

This paper uses Landsat time-series data to examine forest rehabilitation at the PT Singlurus Pratama coal mine in East Kalimantan, Indonesia **(**figure 5**).** The province is the most heavily mined region of the country that itself is the second-largest coal exporter in the world (Woodbury and Arbainsyah, 2020).

In developing nations, surface mining is responsible for 7% of deforestation. It happens in rocks near the Earth's surface, where minerals are most easily obtained. To allow for the removal of the resource, any vegetation, soil, and rocks that overly the mineral seam must be removed. This substantially damages topsoil making regrowth of the vegetation extremely difficult (Woodbury et al, 2019).

The island of Kalimantan (Borneo) is one of the world's richest biodiversity hotspots. And its moist tropical forests are highly diverse and exist on highly weathered but nutrient-poor soils (Fuller et al, 2010). These forests are the most common terrain type where mining occurs in East Kalimantan (Woodbury et al, 2019) (figures 1 and 5). As of 2020, there were 630 left behind surface coal mines in the province. Indonesian law requires mining pits to be filled after extracting minerals; however, these regulations are often violated. With time deep coal mining pits fill up with acidic water, which threatens the local environment and human life (Muslim, 2017; ELTI, 2012). Consequently, the successful rehabilitation of mining sites is critical.

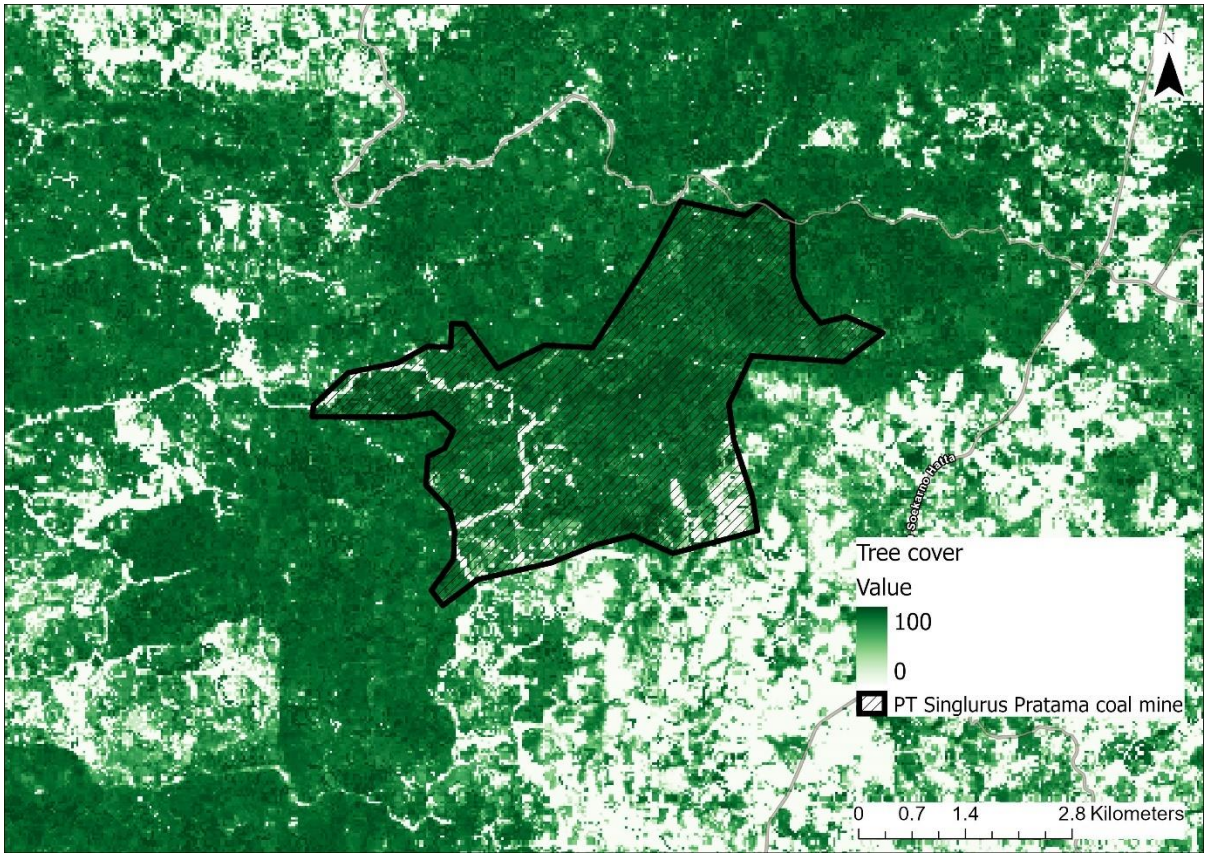

Figure 1. Forest NDVI values around PT Singlurus Pratama coal mine (darker polygon) obtained from Google Earth Engine using Hansen global forest database for 2000 (Hansen et al, 2013). Code link 1 in the code section.

The most accurate monitoring methods estimating forest damage and regrowth are field surveys. In the area of our interest, they very completed by Woodbury et al in 2019. However, such efforts are time-consuming and not always practical as certain sites are inaccessible. On the other hand, remote sensing allows for more frequent imaging, simpler access, and larger-scale monitoring, making it one of the most important global data sources for identifying environmental changes (Hereher, 2015; Kraemer et al, 2015). The moderate resolution of freely available USGS Landsat data makes them appropriate for monitoring changes in forested areas (Woodcock et al, 2008). Moreover, the use of LandTrendr makes it possible to separate long-term from short-term land-use changes with high confidence (Ying et al, 2018).

This study is based on the Landsat collection of 30 m resolution satellite images of Earth, which have been continuously acquired at least every 16 days since 1984 (USGS, 2022). Landsat rich image archive is popular for vegetation trend analysis as it provides accessible, high-quality data for Earth surface monitoring (Bright et al, 2019; USGS, 2022).

The Landsat images were analysed using LandTrendr, a 'Landsat-based detection of Trends in disturbance and recovery' (Kennedy et al, 2012, p.119). LandTrendr uses spectral-temporal segmentation algorithms to capture important features in noisy time series of satellite imagery and generate trajectory-based spectral time series data (Braaten and Kennedy, 2022). These algorithms smooth out undesired random noise caused by natural variations in phenological conditions of vegetation (Kennedy et al, 2012). LandTrendr identifies breakpoints in an image time series between periods of relatively steady spectral trajectory. These breakpoints are referred to as vertices (Bright et al, 2019). The result is a simplified visualisation of a single pixel's spectral trajectory (Kennedy et al, 2010) that allows producing maps of disturbance (figure 2). Based on the trajectory line, each segment can be described by the starting year of disturbance, total duration of the event, and amount and direction of spectral change (Kennedy et al, 2012).

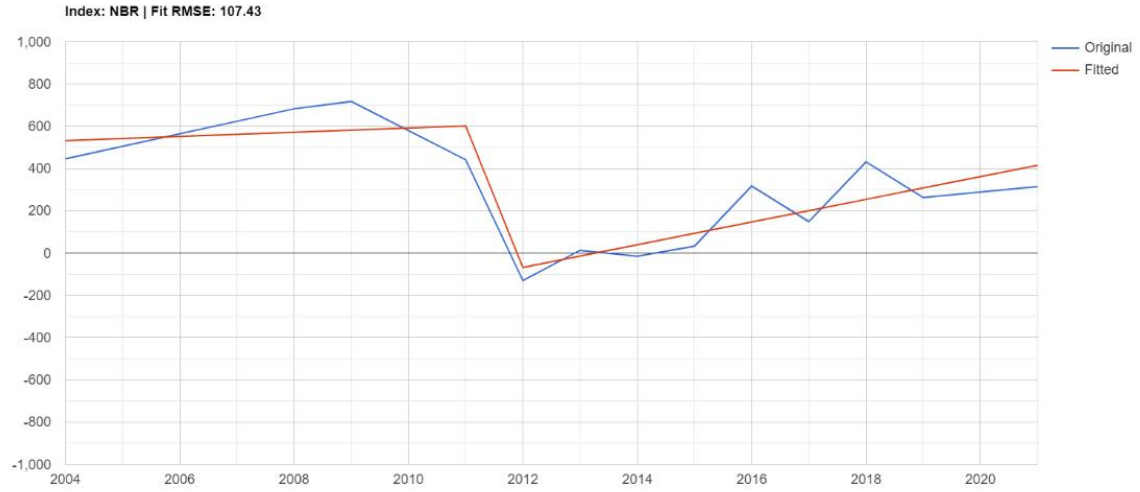

Figure 2. Normalised Burn Ratio (NBR) values for a pixel with a high disturbance at PT Singlurus Pratama coal mine.

LandTrendr algorithms typically calculate a single detection index at a time. We created forest loss/gain maps using the Normalised Difference Vegetation Index (NDVI) for this study. This index was the most responsive to vegetation disturbance as checked in UI LandTrendr Pixel Time Series Plotter, and it is frequently applied to indicate vegetation greenness (Fornacca et al, 2018). NDVI is used to identify vegetation health by measuring the difference between the near-infrared reflectance (NIR) and the visible red band (Red) (figure 3) (Lanorte et al, 2017).

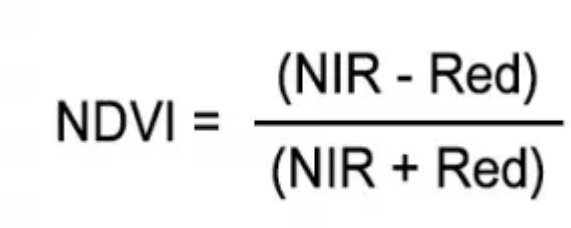

Figure 3. Normalized Difference Vegetation Index (NDVI) formula. Adopted from Lanorte et al, 2017.

Therefore, our overall goal was to use LandTrendr with Landsat time-series in Google Earth Engine (GEE) to detect forest disturbance and regrowth at the PT Singlurus Pratama mine site. We analysed a conceptual model of the spectral feature trajectories to show forest loss and gain trends.

To our knowledge, no English language study has mapped forest recovery of the area where PT Singlurus Pratama mine is located. Thus, this study aims to produce the mapped extent of the regions where afforestation was the most successful and areas where more rehabilitation efforts are needed.

2. Methodology

2.1. Overview

This study follows the landscape disturbance method using LandTrendr. Maps were created of annual forest disturbance and regrowth between 2006 and 2021 for all lands within the boundary of the surface coal mine site (figures 5 and 7). The project utilises continuous quantitative data obtained from Landsat collection and carries out multi-temporal data analysis by extracting key characteristics of simplified spectral trajectories developed with the LandTrendr algorithms in GEE (Kennedy et al., 2010). Maps were created to explain where and how forest loss changed between 2006 and 2021 and where and how post-disturbance forest regrowth was the most successful (figure 4).

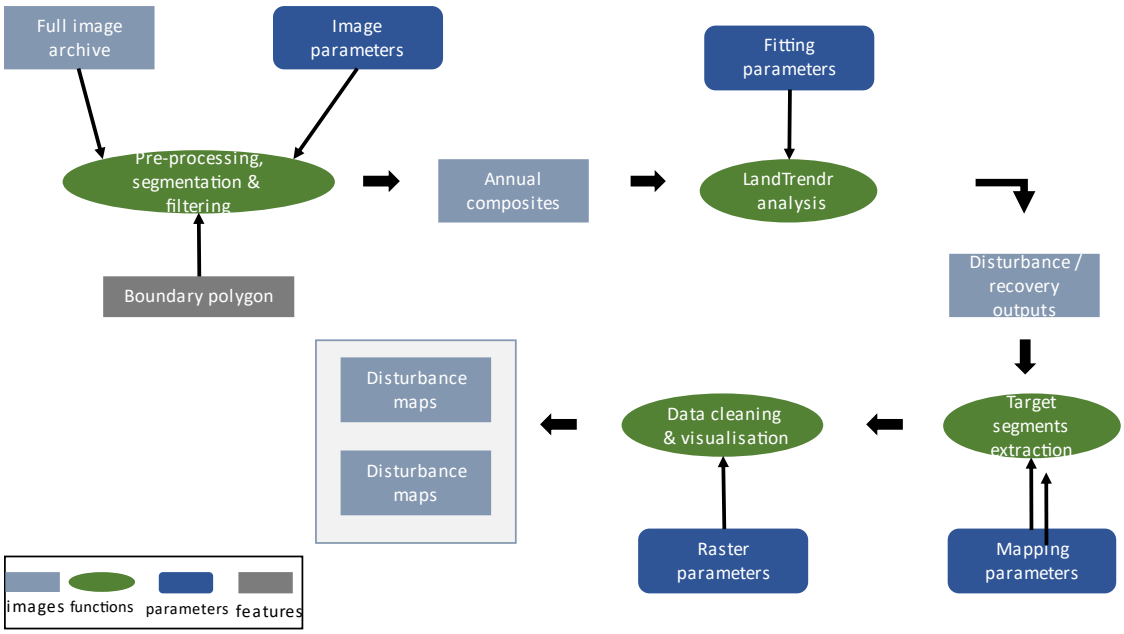

Figure 4. Flowchart for developing disturbance and recovery maps using LandTrendr.

2.2 Study location

The PT Singlurus Pratama coal mine is located in Samboja, Kutai Kartanegara regency, East Kalimantan province, Indonesia, at 1°01'34.5"S 116°56'08.1"E **(**figure 5**).** The forest that was removed for the mine was a mixed dipterocarp forest, which is common in Southeast Asian rain forests and is one of the world's most diversified forest ecosystems (Sheoran et al, 2010).

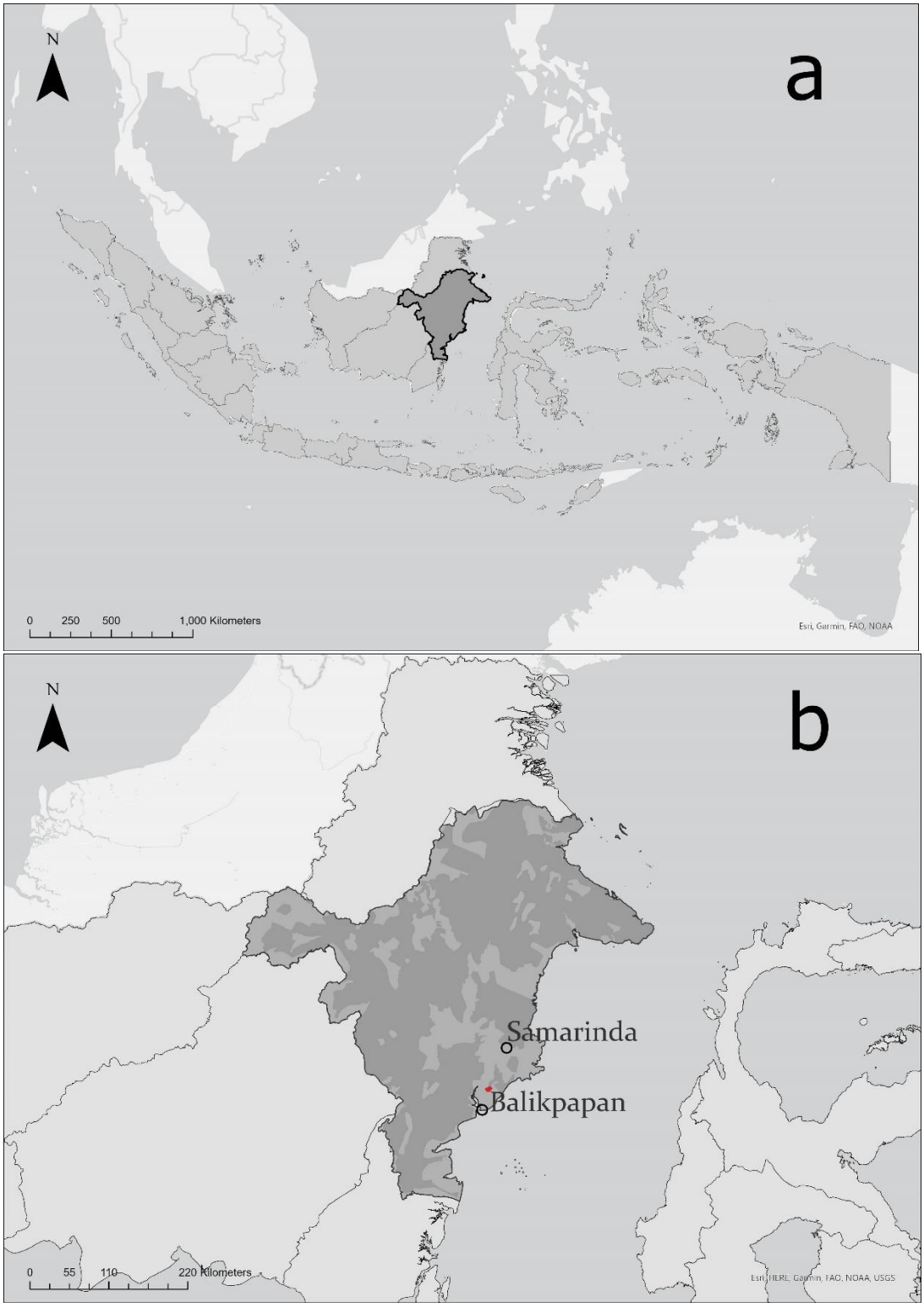
N
a
0 250 500 1,000 Kilometers
Esri, Garmin, FAO, NOAA
N
b
Samarinda
Balikpapan
0 55 110 220 Kilometers
Esri, HERE, Garmin, FAO, NOAA, USGS

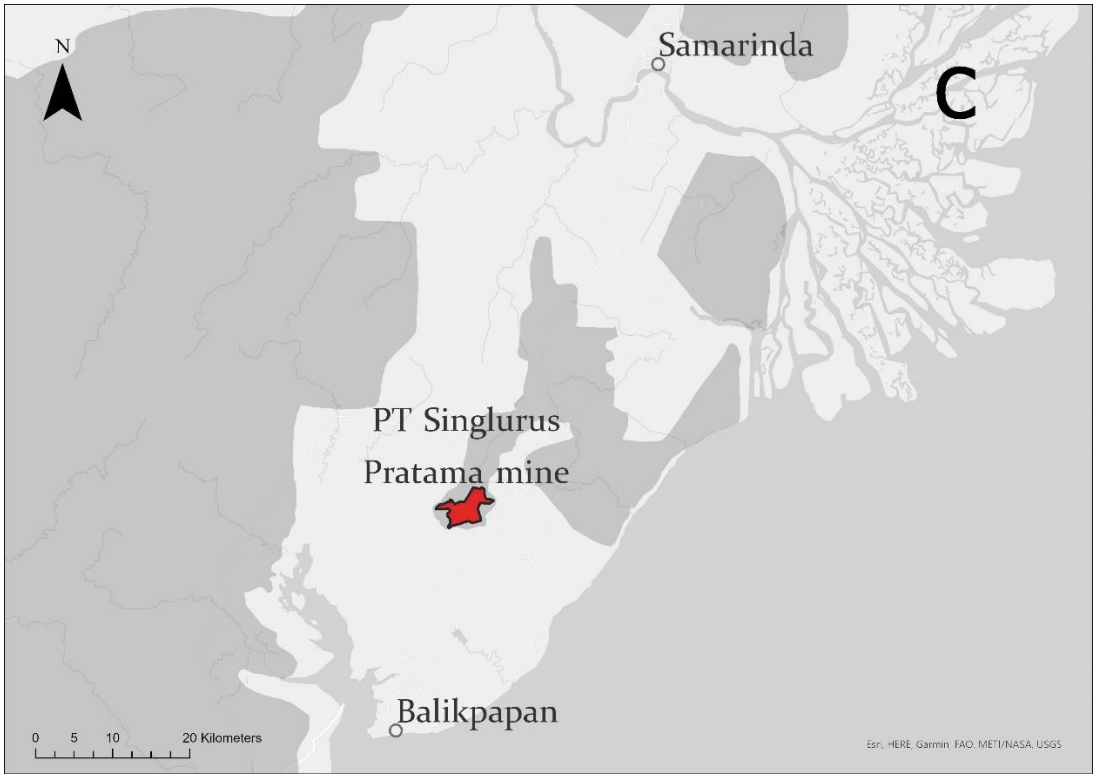

Figure 5. Location of the PT Singlurus Pratama coal mine and East Kalimantan province in Indonesia. Darker grey areas on figures' b' and 'c' represent logging concessions.

The average annual rainfall is 2,250 mm at the site, with a rainy season that spans from December to May **(**figure 6**).** The driest month is August, with 164 mm of rain (Climate-Data.org, 2022).

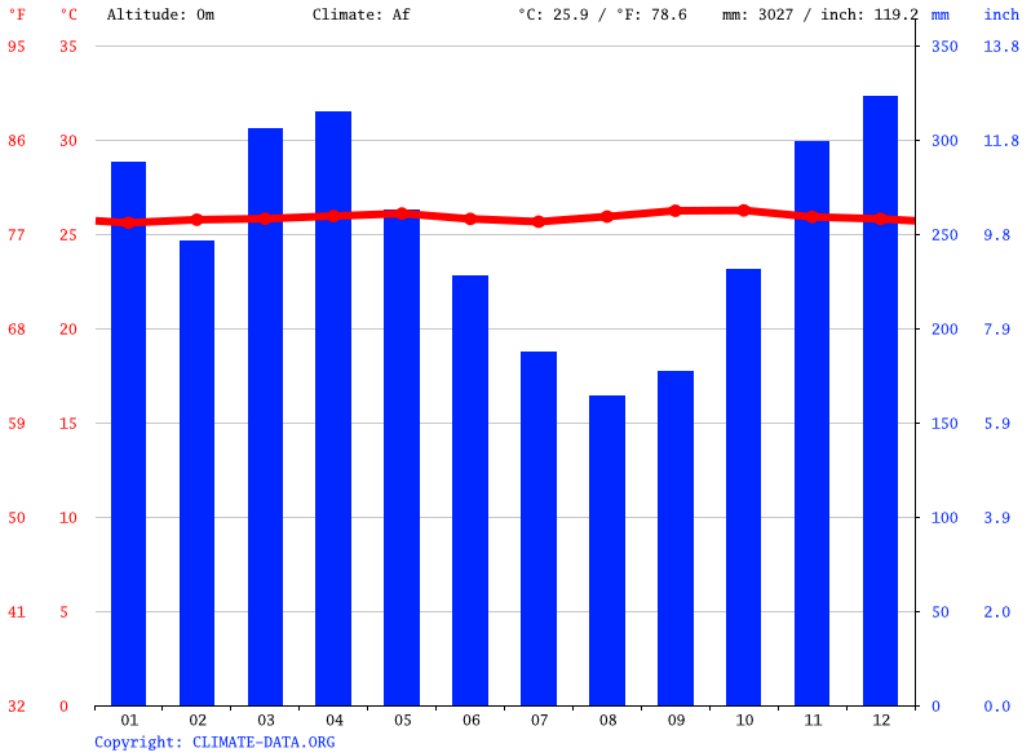

Figure 6. The average monthly rainfall for Kutai Kartanegara regency (Climate-Data.org, 2022).

The coal mine site lies in the hilly area with the highest elevation of 190 meters. The closest large city is Blikpapan, which is 25 km to the south, and the provincial capital, Samarinda, is 65 km to the north. From these cities, the coal is usually exported to other provinces and countries. A rain forest currently surrounds the site, and PT Singlurus Pratama is obliged to restore native forest, which they began to do in 2009 (Woodbury et al, 2019).

Figure 7. Boundary polygon of the PT Singlurus Pratama coal mine (Google, 2022).

2.3. LandTrendr pre-processing, segmentation and filtering

The data for this study was obtained from Landsat data collection using Google Earth Engine (GEE). The boundary polygon of PT Singlurus Pratama coal mine site was manually created in ArcGIS Pro and uploaded into GEE as a shapefile. The polygon was based on the maximum visible surface mine disruption extant of the forested area manually identified using Google Earth Pro **(**figures 7 and 9**).** The total area of the polygon is 16.29 km2; this number was used as an estimated total area of the PT Singlurus Pratama mine site.

2006 was chosen as a starting year for this analysis based on historical imagery available in Google Earth Pro and on time series plots created with UI LandTrendr Pixel Time Series Plotter. Little to no mine related disturbing was identified prior to 2006 **(**figures 8 and 9**).** The available English language literature on the topic also estimates 2006 as the starting year of PT Singlurus

Pratama coal extraction (Woodbury et al, 2019).

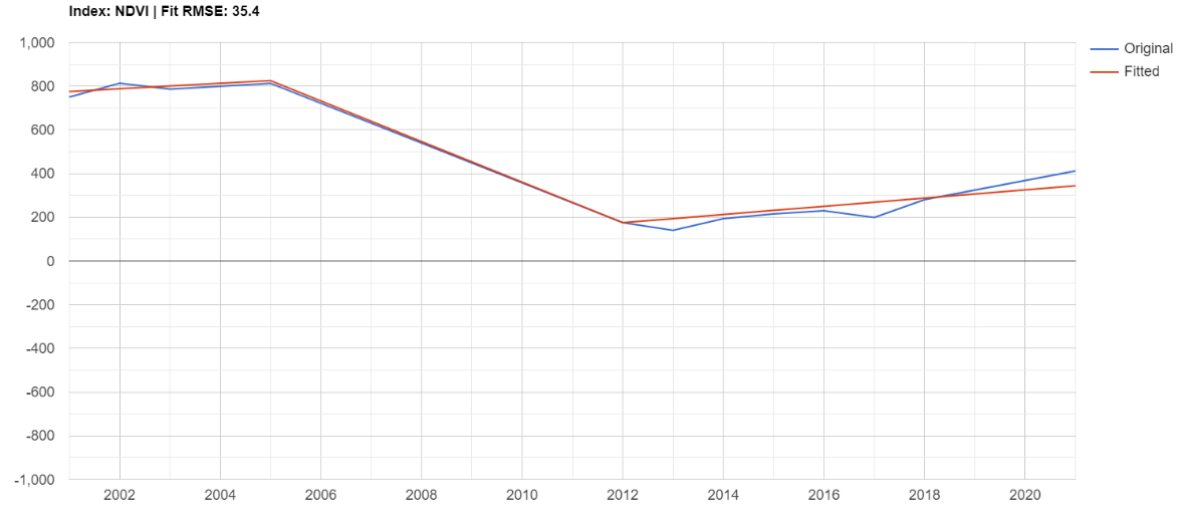

Figure 8. Time-series values for a pixel with relatively high forest disturbance in PT Singlurus Pratama coal mine site (UI LandTrendr Pixel Time Series Plotter).

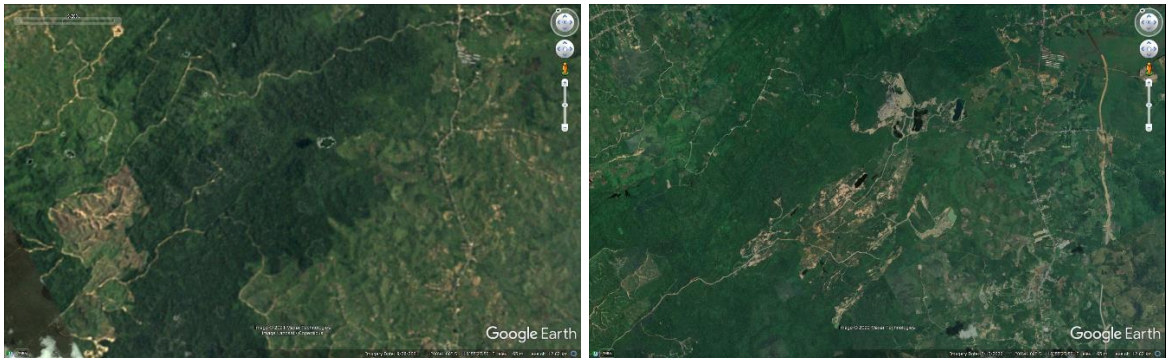

Figure 9. The location of the PT Singlurus Pratama coal mine site in 2001 (left), and the same area in 2021 (right) (Google, 2022).

The data were analysed for each year between June 1st and October 31st. Image dates were chosen when rainfall and clouds are minimal in the region (figure 2), but forest vegetation and sunshine is maximised (figure 5).

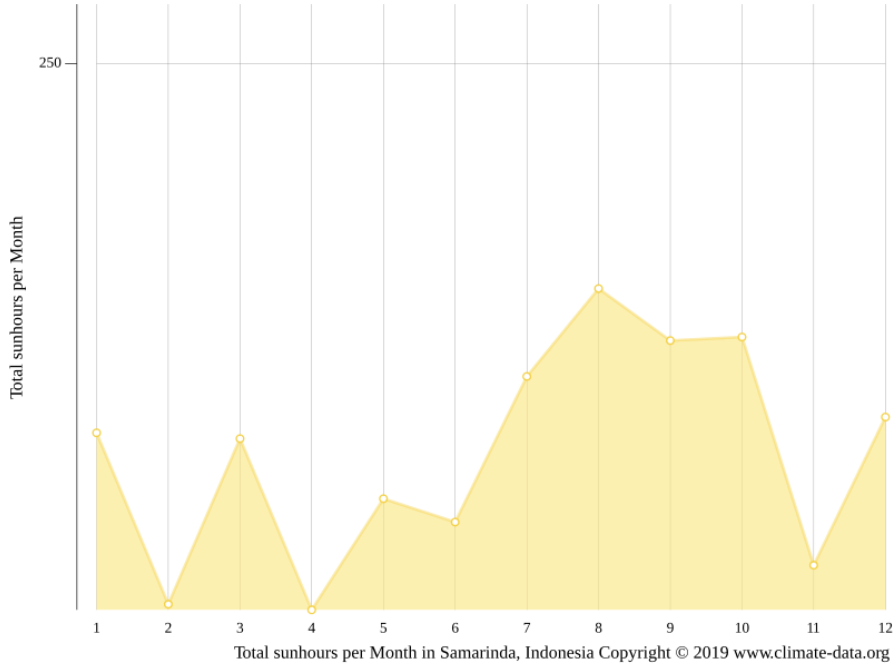

Figure 10. Total hours of sunshine in Samarinda, East Kalimantan by month (Climate-Data.org, 2022).

As explained above, the Landsat images were extracted using the GEE implementation of LandTrendr. First, values for both NDVI and NBR (Normalised Burn Ratio) indices were extracted, as they were the most responsive to vegetation disturbance as checked in UI LandTrendr Pixel Time Series Plotter. However, even though both indices showed similar gain/loss trends, their values did differ substantially in areas where post-mine lakes were formed. Whereas NDVI values dropped significantly NBR values did not show any serious change and, in some cases, even increased (figure 11). As most of these artificial lakes were not in the area before the coal extraction, we decided to use only NDVI values to determine forest loss/gain patterns (Xu et al, 2019).

Figure 11. NDVI and NBR values for a pixel where artificial lake was formed after surface mining (1°01'34.5"S 116°56'08.1"E).

We started LandTrendr analysis with pre-processing, segmentation and filtering. Each pixel was matched with cloud, shadow, and water masks. As the LandTrendr algorithms allow image mosaicking from the best available pixels within the specified season, completely cloud-free images were not required (Kennedy et al, 2010). When several images for a given year were available, the data closest to the median was preferred. If the pixel was masked, the nearest pixel value was used. Next, the segmentation algorithms analysed the time series of these source data. The algorithms' parameters were set based on prior similar research in the literature (Kennedy et al, 2018) (figure 12). The segmentation process resulted in identification of start and end years of disturbance and the best trajectory line.

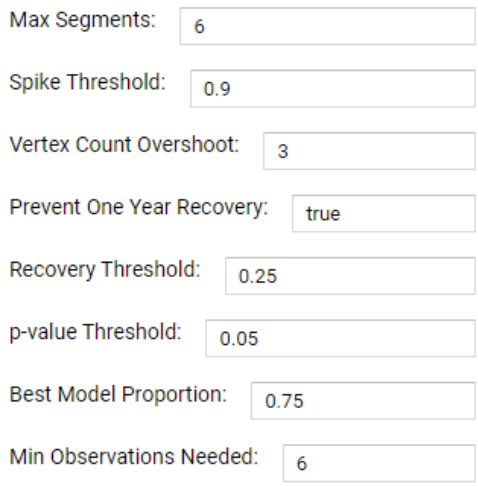

Figure 12. LandTrendr segmentation parameters.

2.4 Developing disturbance and regrowth maps

To develop disturbance maps, the delta was defined. It is a parameter to determine what segments to return information about. It was set to 'loss' to produce forest loss outputs and 'gain' to obtain regrowth values (Braaten and Kennedy, 2022). Then the type of change (sort) to identify if there was more than one change event in a pixel time series was set to 'greatest' for loss and gain analysis.

Next, the disturbance was determined to show either decline or increase in NDVI values per pixel (Kennedy et al, 2010). The magnitude of disturbance for each segment was defined as the difference between the computed vegetation cover values of the initial and ending vertices (Kennedy et al, 2012) (figure 13a). The NDVI delta threshold was set to be larger (>) than 0.3 (300) for the 'loss analysis' and larger than 0.2 (200) for the 'gain analysis'. These values were assigned by trial and error, as setting the gain threshold to 0.3 resulted in fewer regrowth pixels.

Then the duration of the disturbance process was defined as the difference between the starting and ending breakpoints (figure 13b). The threshold for the number of years a change event took to complete was set to be smaller than five years. The year of disturbance was defined as the first year after starting of the segment. If the data for this first year was absent due to clouds, the next valid year was used instead. The change event was filtered by pre-change NDVI value by applying 'preval' to be larger than 0.4 (400). After this, the minimum mapping unit (mmu) was defined to be at least 11 pixels in size. This size is small enough to capture forest activities but large enough to avoid mapping 'noise' (Kennedy et al, 2012).

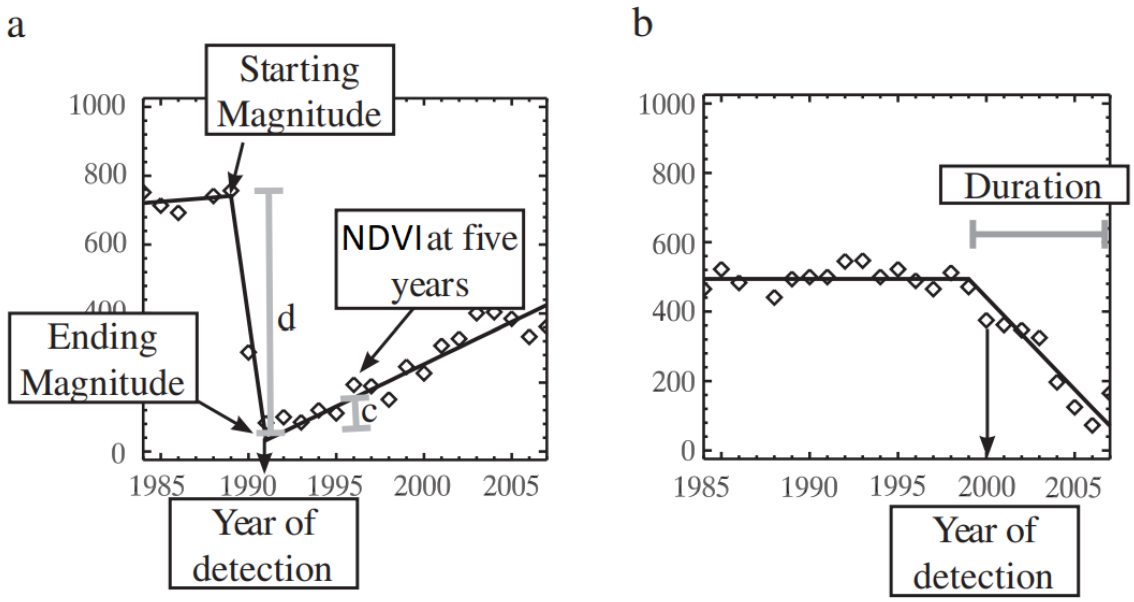

Figure 13. Disturbance and regrowth NDVI values from segmented trajectories. Adopted from Kennedy et al, 2012, p. 122.

Finally, disturbance maps for forest loss and gain were created from the yearly magnitude and duration images. These maps included three layers of information: year of disturbance duration, the magnitude of disturbance, and duration of disturbance change (Braaten and Kennedy, 2022). Then the histogram charts were produced in GEE for all these layers. They helped to visually quantify the change for each layer by comparing frequency (number of detected pixels) to values**.**

As the next step of our analysis, the disturbance and recovery maps were exported to Google Drive as tif images. These maps: three for forest loss (year of disturbance, magnitude, and duration of change) and three for forest gain were uploaded into ArcGIS Pro for further analysis.

In ArcGIS Pro, 'Raster calculator' was used to clean the null values using the 'condition' command:
Con("Bukit_Magnitude_NDVI_loss4.tif"!=0,"Bukit_Magnitude_NDVI_loss4.tif").
Next, loss magnitude values were subtracted from gain values to visualise the general situation with regrowth relative to forest loss (figure 14).

Raster images for duration and year of change were also reclassified to make visual detection of general trends easier. Zonal statistics was used in order to calculate the total area of loss and the total area of gain (table 1). Finally, polygons were created to highlight areas where afforestation was most successful and areas where more forest rehabilitation efforts are needed (figure 24).

Results

Average forest gain NDVI values were calculated to be at 367.3, with values ranging from 200 to 654. The highest recovery was detected in areas that bordered heavily mined lands. These lands, where topsoil has been removed, show little to no NDVI increase (figure 16). Pixels taken from areas with the highest forest gain NDVI values show similar trends of regrowth after 2015 (figures 16a, 16b, 16c).

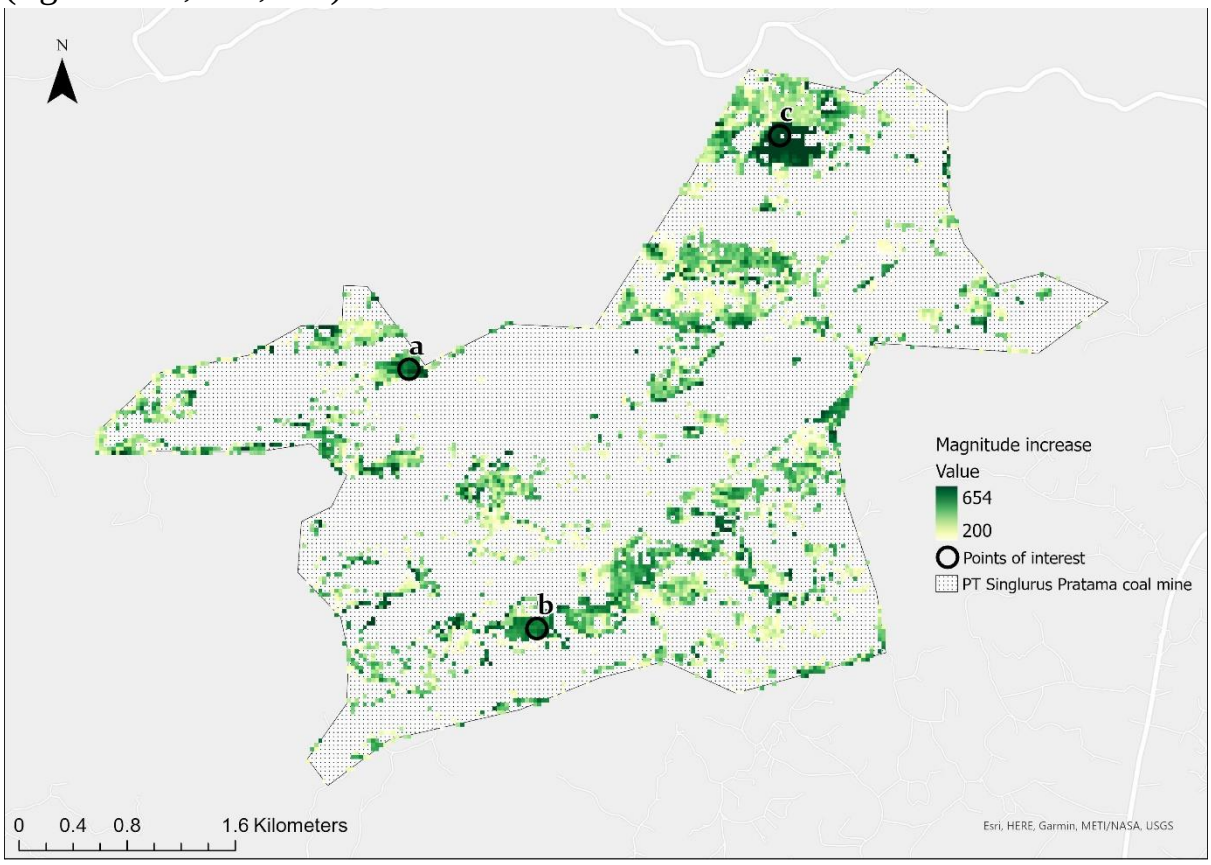

a

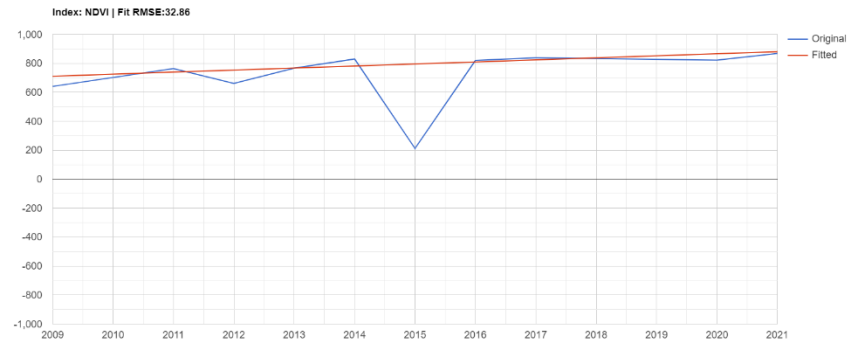

b

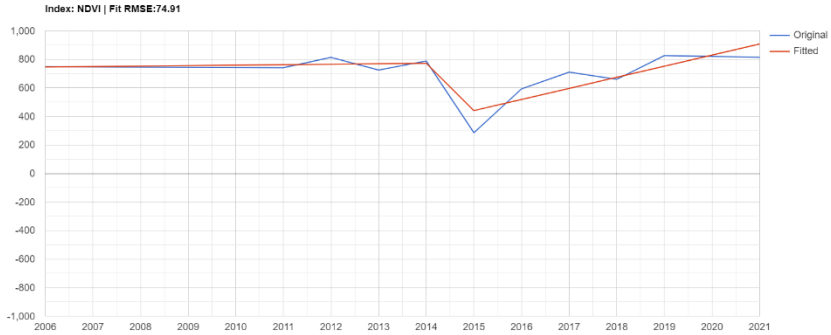

c

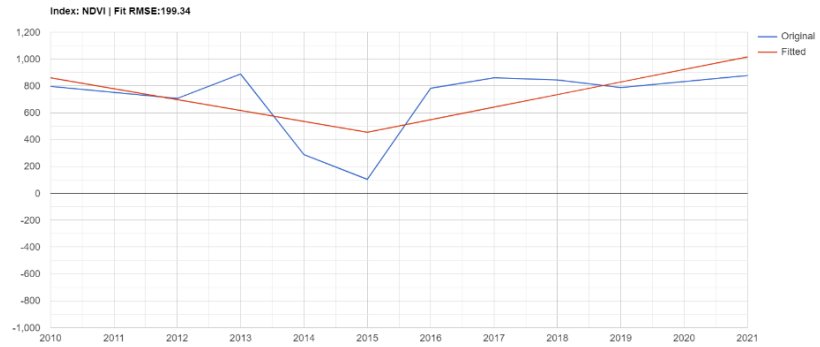

Figure 16. NDVI recovery magnitude values of the site where PT Singlurus Pratama coal mine is located. Figures a, b, c represent NDVI values from segmented trajectories of three pixels with high recovery. a) Recovery segments lasting one year. b) and c) Recovery segments lasting more than one year. Code link 2 in the code section.

The average magnitude decrease was at 526.8. The forest loss NDVI values ranged between 300 and 1179 (figure 17). Most areas with a high magnitude decrease in NDVI values were visible with a naked eye on Google satellite images as of 2021 (figures 7 and 9). Artificial lakes were formed in areas where the disturbance was higher than 1000. Some of these lakes were temporal and allowed for vegetation to slowly recover (figure 17a); some, however, are still filled with water, and recovery shows a negative trend (figure 17b).

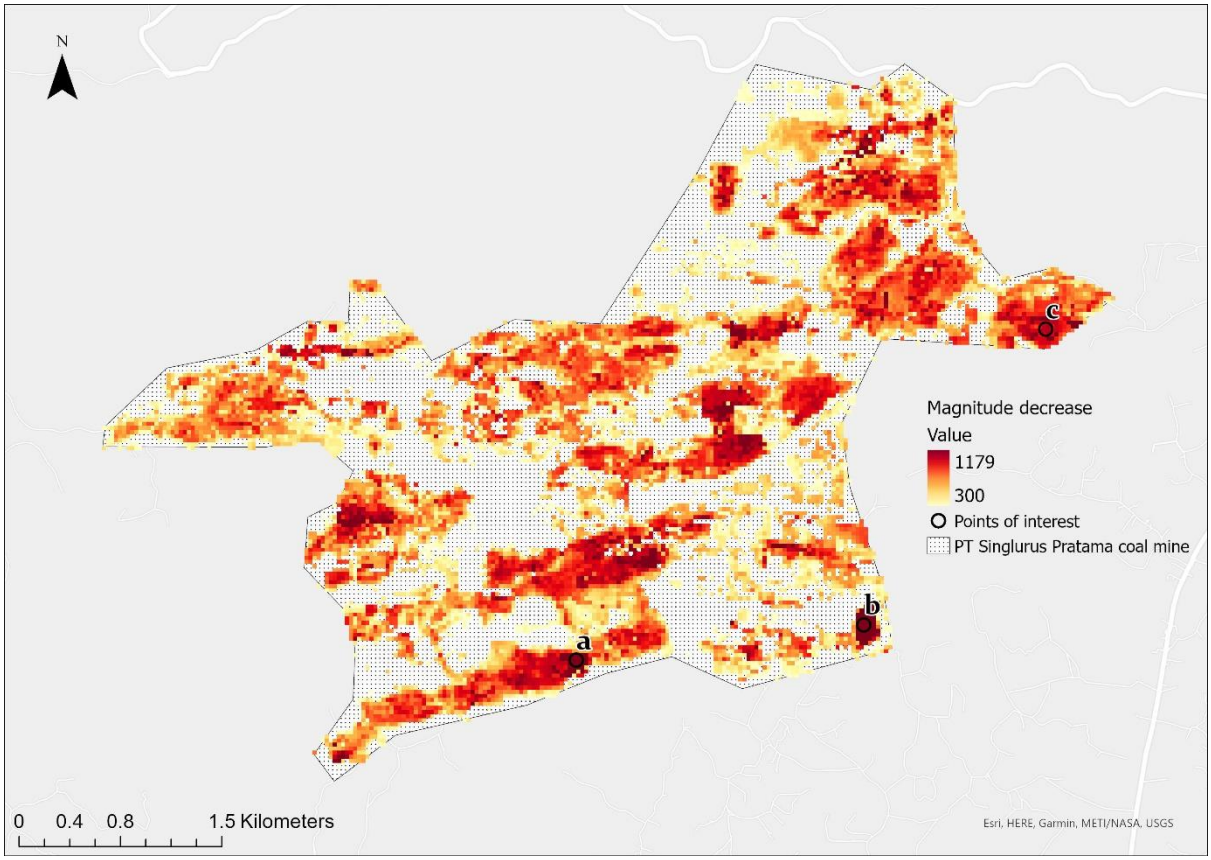

a

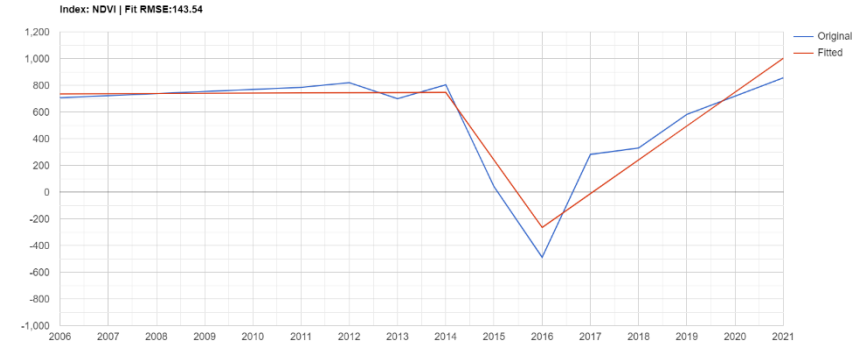

- Year: 2015
- Magnitude: 1012
- Duration: 2
- Pre-value: 747
- Rate: 506

b

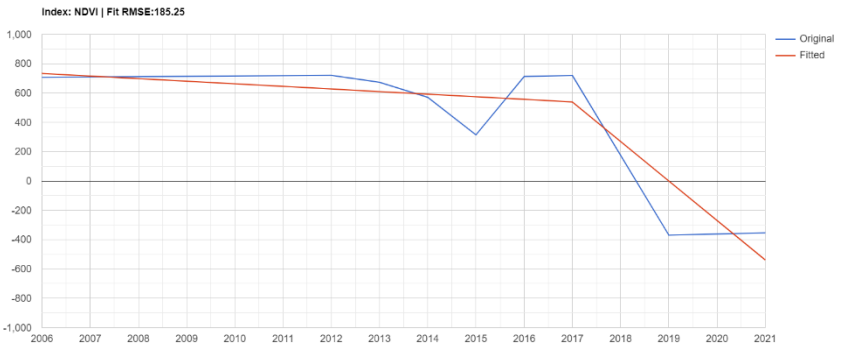

- Year: 2018
- Magnitude: 1078
- Duration: 4
- Pre-value: 539
- Rate: 269

c

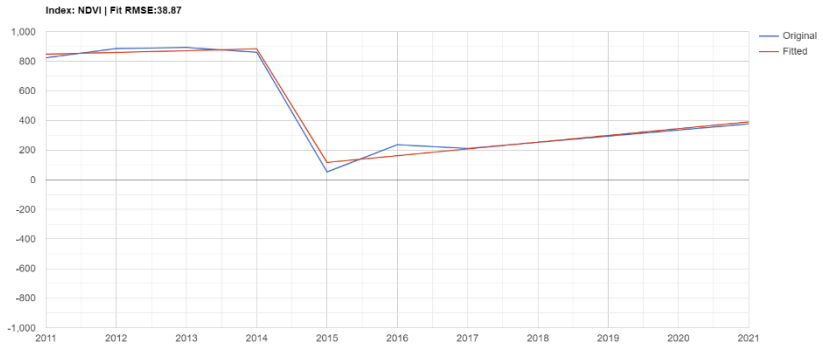

- Year: 2015
- Magnitude: 767
- Duration: 1
- Pre-value: 884
- Rate: 767

Figure 17. NDVI disturbance magnitude values of the site where PT Singlurus Pratama coal mine is located. Figures a, b, c represent NDVI values from segmented trajectories of three pixels with high disturbance. a) Disturbance segments lasting two years. b) Disturbance segments lasting four years. c) Disturbance segments lasting one year. Code link 3 in the code section.

The total area of forest disruption, calculated by the substruction of loss magnitude values from gain magnitude values, resulted in much larger areas where forest loss values were more significant than regrowth values (table 1).

Table 1. Relative total area of highest forest recovery and disturbance from 2006 to 2021.

	Area in km2	Per cent
Gain > loss	1.0017	6.14 %
Loss > gain	8.5230	52.32%
No significant change detected	6.7653	41.54%

The same results were visualised below (figure 14), where forest loss and gain magnitude values were generalised for a more straightforward interpretation.

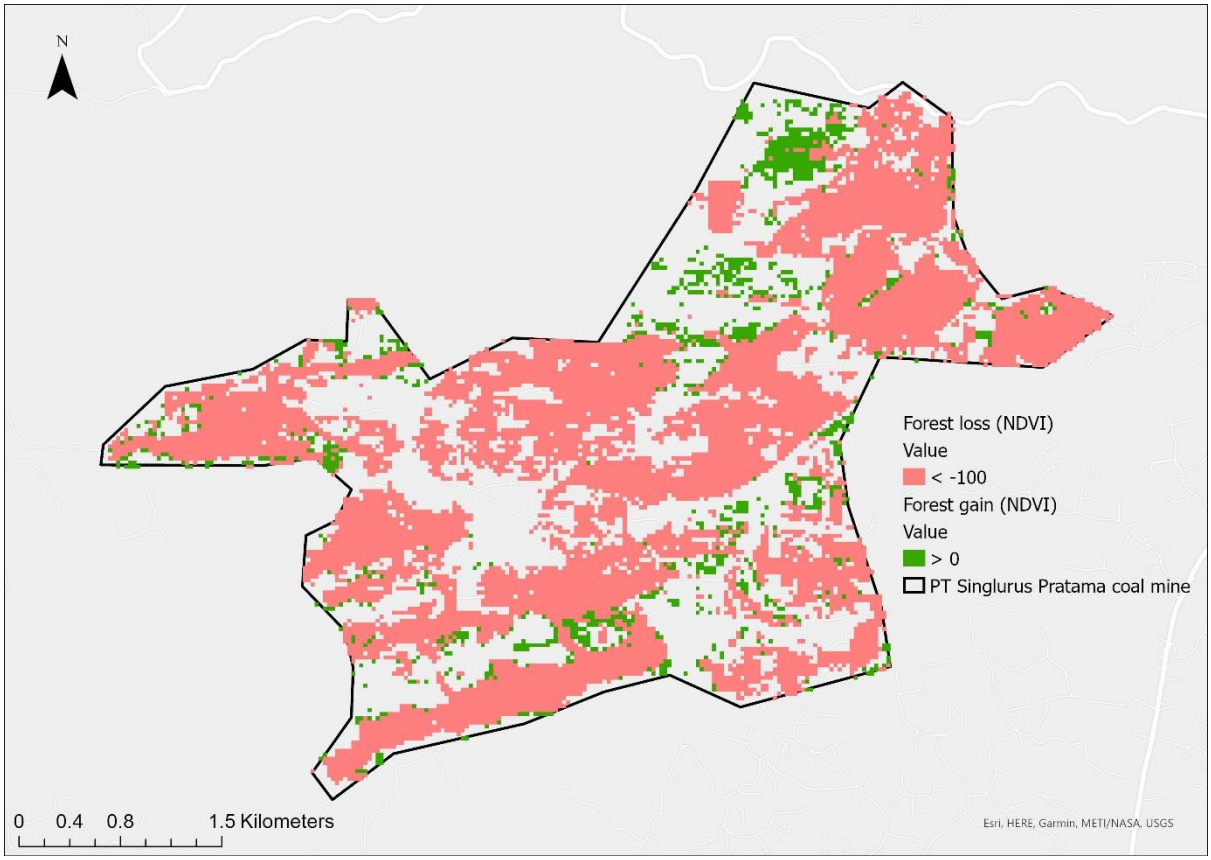

Figure 14. Relative total area of highest forest recovery and disturbance for the PT Singlurus Pratama coal mine over period from 2006 to 2021.

However, the general trend for the coal mine site was positive, as from around 2015, the NDVI values steadily increased (figure 15). These results were confirmed by the year of change charts below, where NDVI decreased after 2011 and increased after 2013 (figure 20).

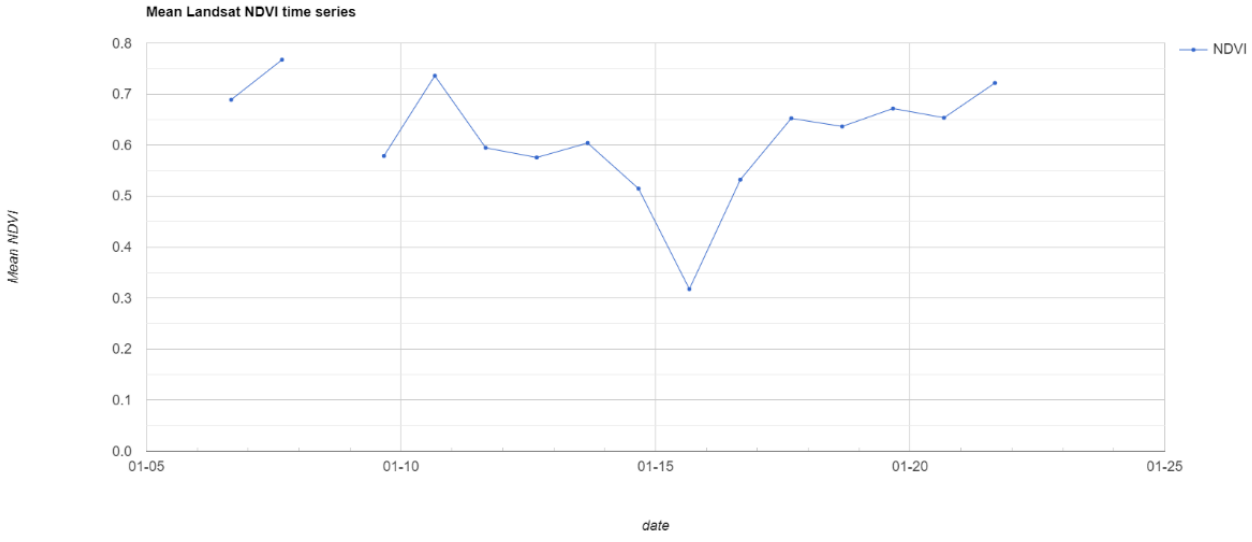

Figure 15. Disturbance and regrowth NDVI values from segmented trajectories for the PT Singlurus Pratama coal mine reclamation area. Code link 4 in the code section.

The spatial and temporal patterns of afforestation and forest loss are rendered in figures 18, 19 and 20. The most common year when the change occurred for the recovery was 2016 (figures 18 and 20). For the forest loss, on the other hand, there appear to be numerous years when the change took place; the most common were 2007 and 2015 (figures 19 and 20). There are pockets of regions spread around the mining site where regrowth took place in similar years. On the other hand, forest loss occurred nearly annually, and there are three visible regions of gradual deforestation. The older one was highlighted in dark purple and has predominantly happened in the centre and western portions of the mining site. In contrast, the more recent deforestation occurred in the southern and north-eastern sections of PT Singlurus Pratama (figure 19).

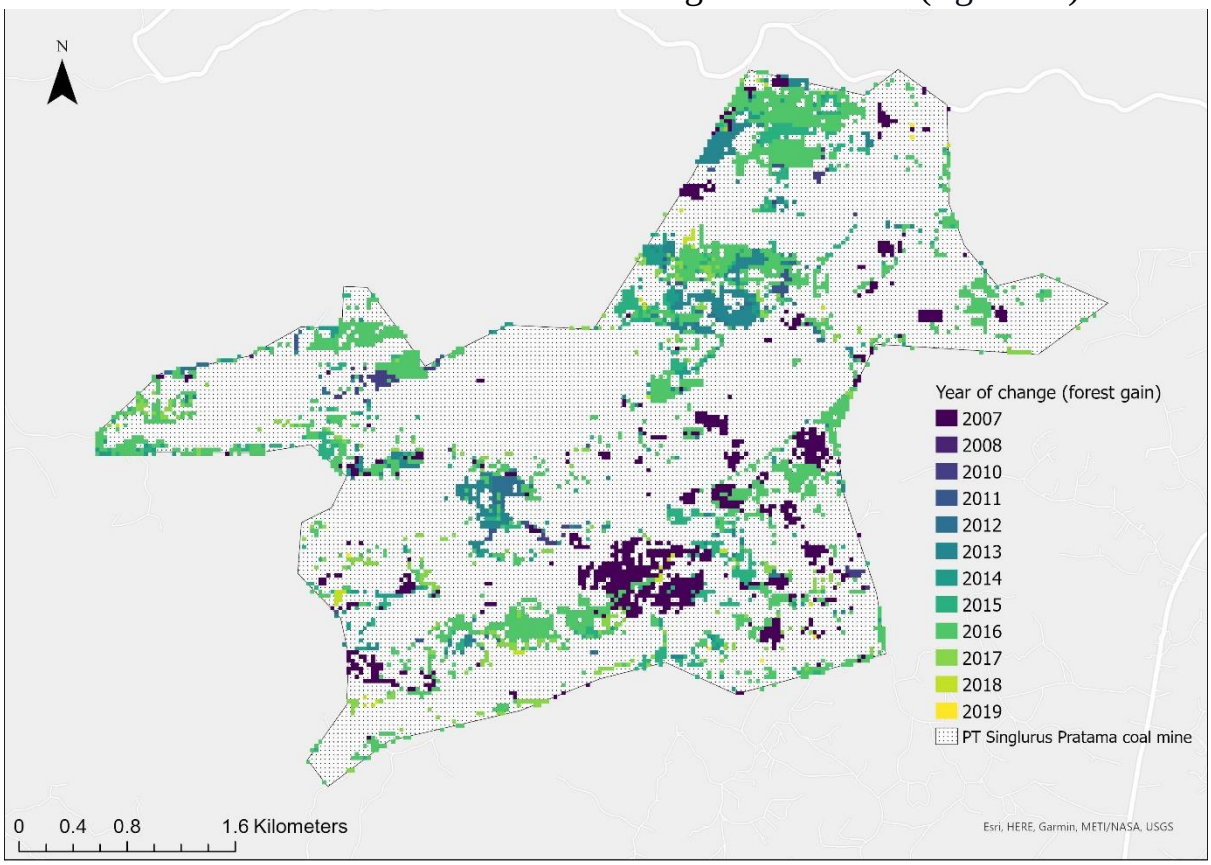

Figure 18. Year of detected forest recovery change at the PT Singlurus Pratama coal mine reclamation area. Code link 2 in the code section.

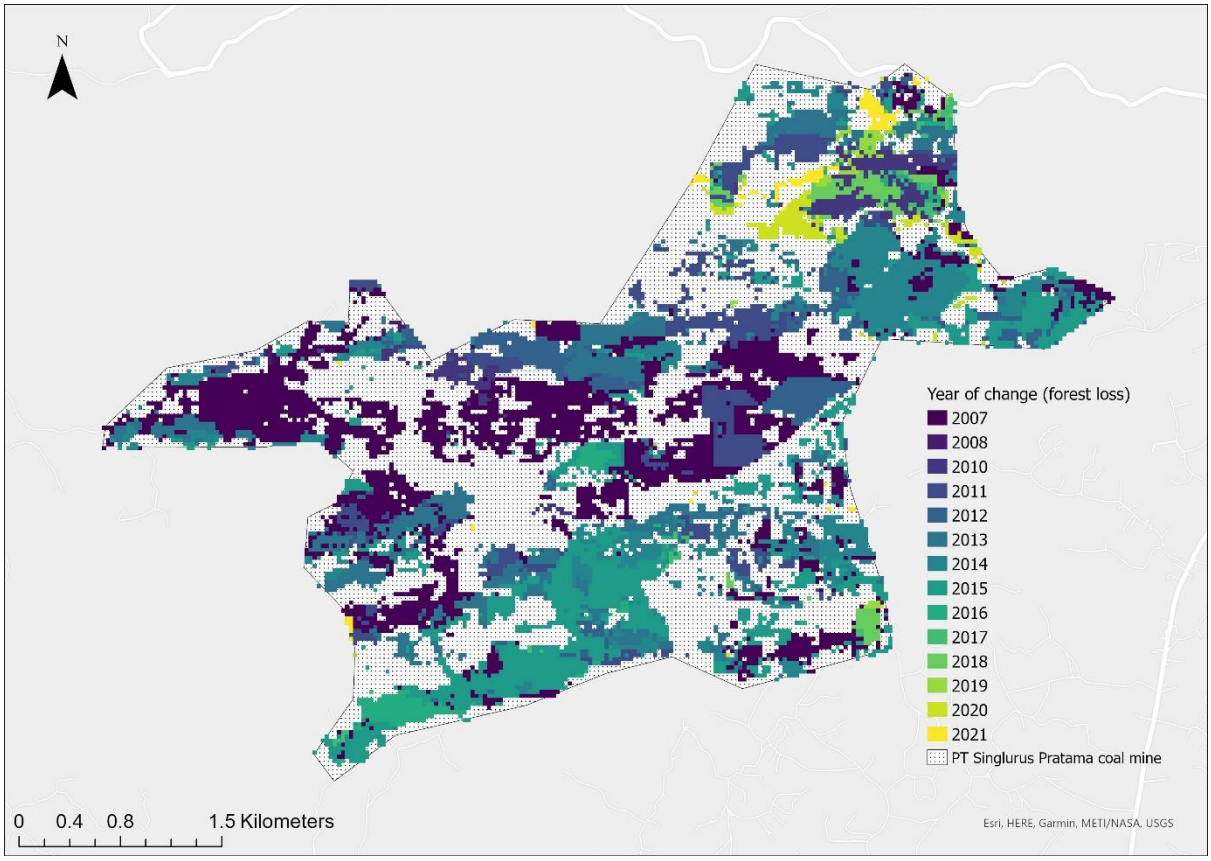

Figure 19. Year of detected forest disturbance change at the PT Singlurus Pratama coal mine reclamation area. Code link 3 in the code section.

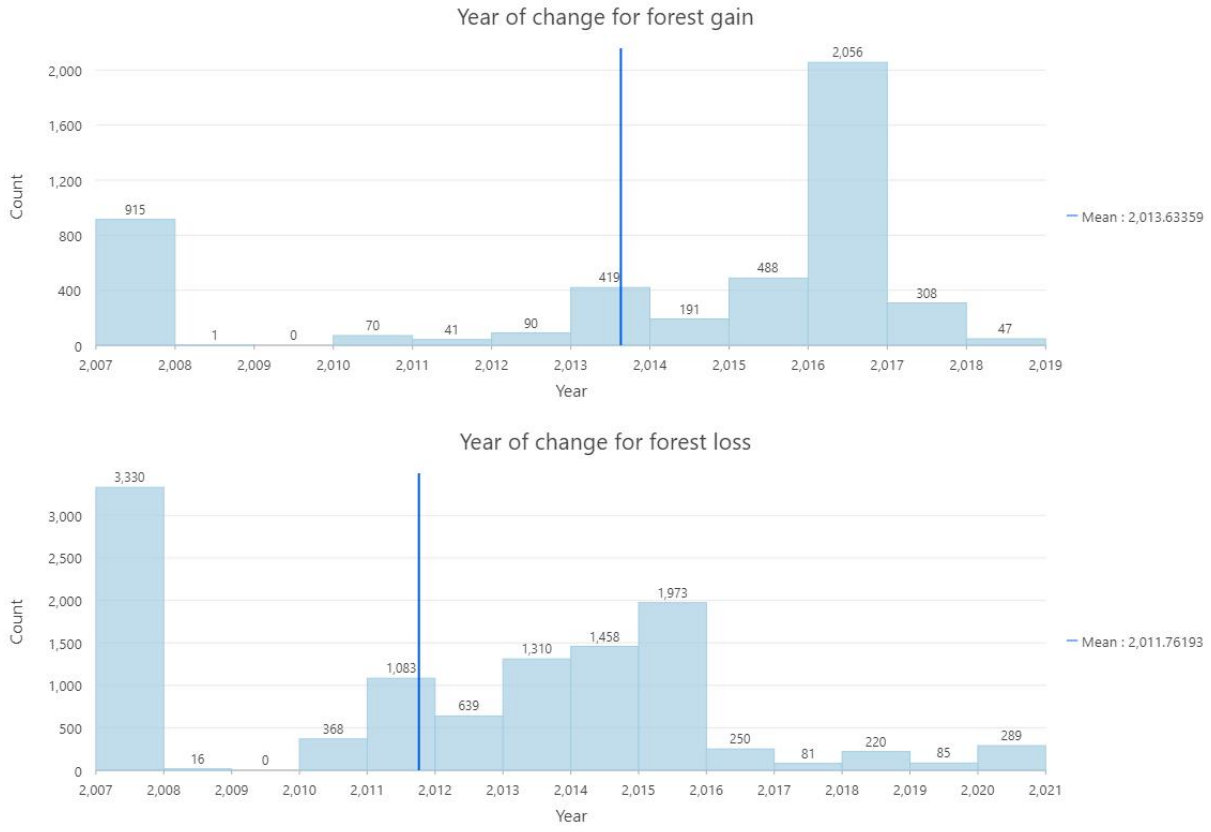

Figure 20. Year of detected forest recovery and disturbance change at the PT Singlurus Pratama coal mine reclamation area.

The duration of gain shows that on average, it took 7.1 years for the regrowth of trees to be noticeable by NDVI values (figures 21 and 23), whereas the duration of forest disturbance was at around four years with more than 50 % occurring in only one or two years (figures 22 and 23). This trend is visible comparing the two maps below.

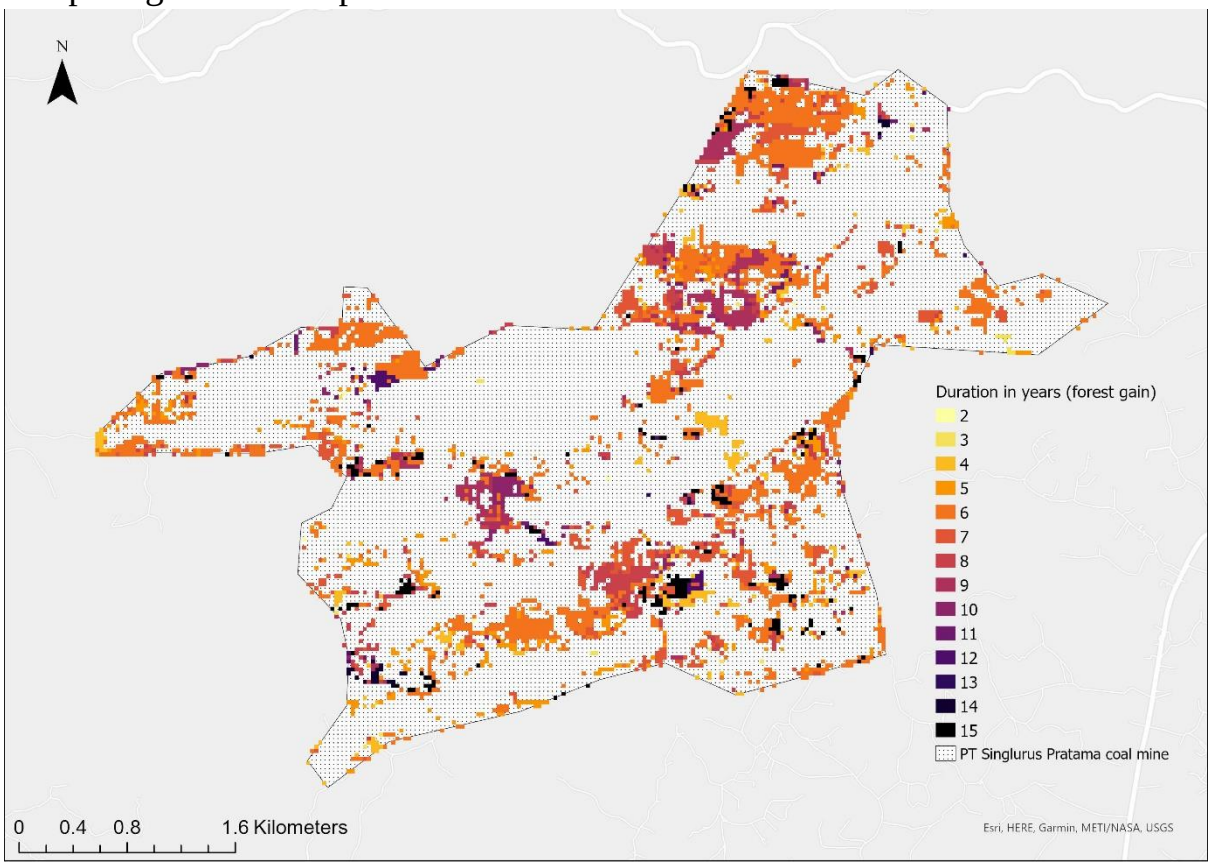

Figure 21. Duration of forest recovery at the PT Singlurus Pratama coal mine reclamation area. Code link 2 in the code section.

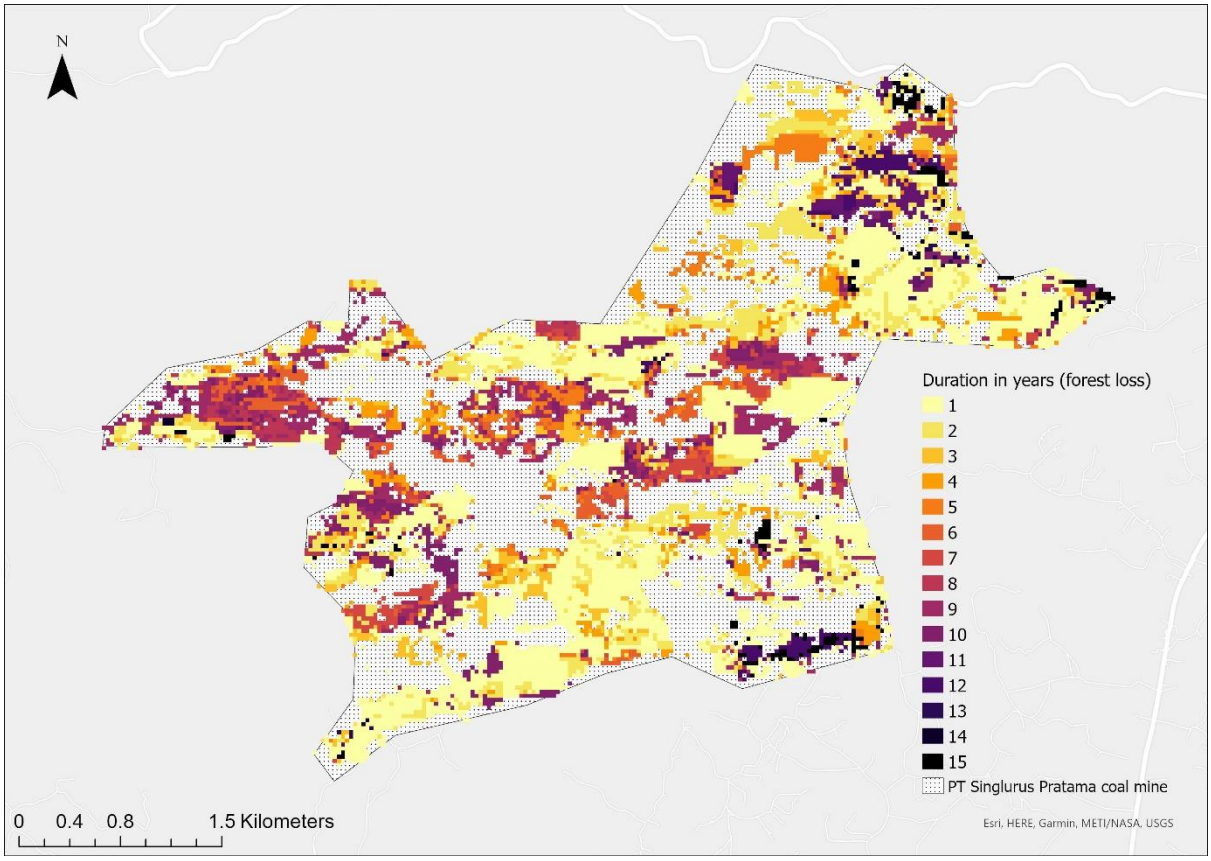

Figure 22. Duration of forest disturbance at the PT Singlurus Pratama coal mine reclamation area. Code link 3 in the code section.

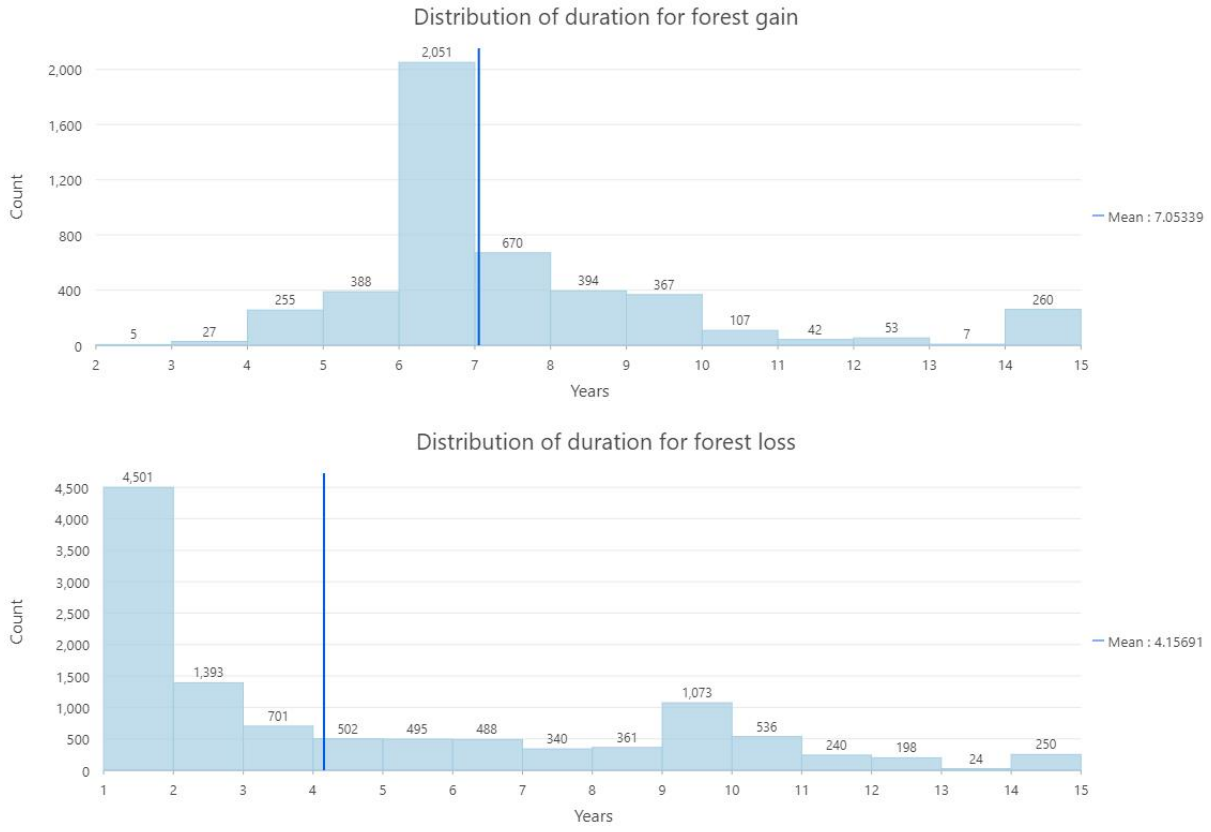

Figure 23. Duration of forest recovery and disturbance at the PT Singlurus Pratama coal mine reclamation area.

Discussion

Accurate information about the timing and extent of forest regrowth is crucial for environmental assessment and policy making (Zhang et al, 2012). Using LandTrendr algorithms with a time series of Landsat data, we were able to map the spatial and temporal characteristics of forest regrowth and loss of the mine site. One clear advantage of Landsat is the availability of consistent data for over three decades, allowing long-term analyses (Schmidt et al, 2016). In this study, data for fifteen years were used as this period corresponds with the time when most of the change occurred.

More research is needed to estimate areas where forest rehabilitation has been successful confidently; however, we identified areas where forest regrowth was the most effective. Those areas had both a high decrease in NDVI values and, later, a high magnitude increase, as shown in figure 24.

Some of these successfully afforested areas, like the 'green corridor' in the southern section and a stand in the centre of the mine site, are confirmed in the literature. Plots planted in 2009, 2011, and 2016 (Woodbury et al, 2019) (figure 25) did show increases in NDVI values in analysis (figure 24). Moreover, it is natural that trees planted in 2009 and 2011 showed the highest increase in magnitude between 2013 and 2018, as was detected using LandTrendr (figure 20).

There are large areas where NDVI values decreased considerably (figures 17 and 24). It is concerning that much of it happened between 2009 and 2016 (figures 19 and 20), precisely after the rehabilitation efforts were in place. Comparison of magnitude loss and gain locations clearly shows that most deforested areas had little forest regrowth. This can be explained by the difficulty of growing trees in areas where topsoil was removed. To complicate this more, it obviously takes more time to regrow forest than to cut it, as indicated in the duration maps where most forest loss happened in one to three

years, but it took on average seven years for the regrowth to occur (figure 23).

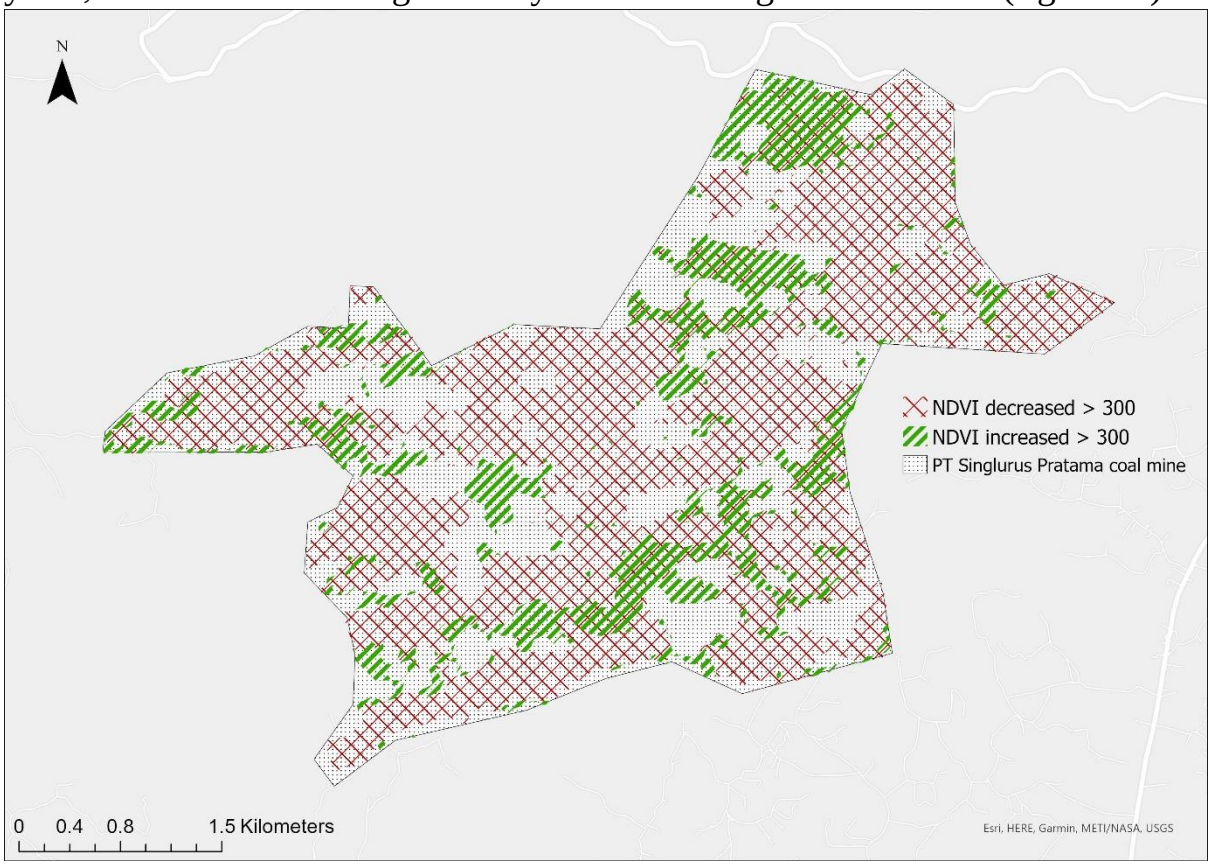

Figure 24. Areas with the highest NDVI recovery and disturbance for the PT Singlurus Pratama coal mine reclamation area over period from 2006 to 2021. Intersected gain/loss areas represent sites with most successful recovery. Red areas represent sites where more rehabilitation efforts are needed.

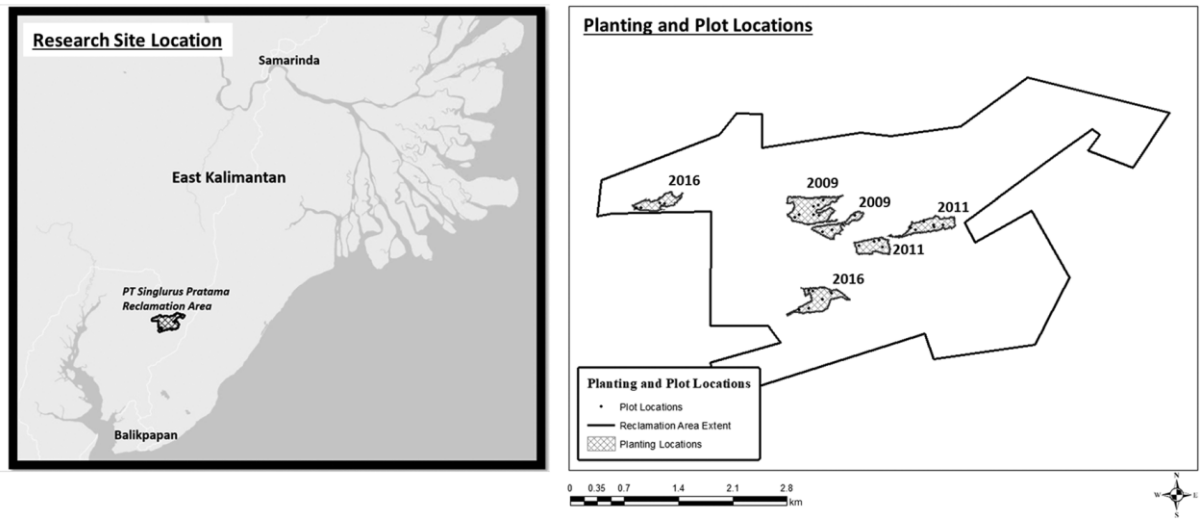

Figure 25. (a) Shows location of the PT Singlurus Pratama coal mine reclamation area in East Kalimantan, Indonesia (01° 000 55.0’, 116° 54’

30.0’). (b) Shows the locations of the plantations and sample plots within the reclamation area extent at PT Singlurus Pratama. Adopted from Woodbury et al, 2019, p.475.

Conclusion and further work

Given more time and data, more robust conclusions about the areas where rehabilitation was most successful and failed could have been made. For example, high magnitudes of loss and regrowth in 2006 and 2007 were not explained (figure 20), as data before 2006 was not analysed, and no mention of mining at the site of interest has been found before 2006 in the literature. However, the results suggest that significant forest loss started to happen before 2006. Post-mining conversion of pits to lakes and their subsequent afforestation possesses another problem, as some NDVI signals were unstable, leading to potentially false trajectories. The accuracy assessment, which was not carried out, could also improve the confidence of the findings.

In general, the afforestation of mining sites is a very important topic of research, and PT Singlurus Pratama reclamation area is likely to receive more scientific interest as the future capital of Indonesia will possibly be constructed in close proximity to this mining site (Clark, 2022).

References

Braaten, J., Kennedy, R., 2022. LT-GEE Guide, API Functions. *Oregon State University*, Available at: https://emapr.github.io/LT-GEE/introduction.html (Accessed: 10 January 2022).

Bright, B.C., Hudak, A.T., Kennedy, R.E., Braaten, J.D., Khalyani, A.H., 2019. Examining post-fire vegetation recovery with Landsat time series analysis in three western North American forest types. *Fire Ecology*, 15(1), pp. 1-14.

Clark, J., 2022. Nusantara – New Capital City of Indonesia. *Future Southeast Asia*, January 18, 2022. Available at: https://futuresoutheastasia.com/nusantara-new-capital-city-of-indonesia/ (Accessed: 19 January 2022)

Climate-Data.org, 2022. Climate Samarinda (Indonesia), *Climate-Data.org*. Available at: https://en.climate-data.org/asia/indonesia/east-kalimantan/samarinda-46950/#climate-graph (Accessed: 4 January 2022)

Cohen, W.B., Yang, Z., Kennedy, R., 2010. Detecting trends in forest disturbance and recovery using yearly Landsat time series: 2. TimeSync — Tools for calibration and validation. *Remote Sensing of Environment*, 114(12), pp. 2911-2924. Available at: Detecting trends in forest disturbance and recovery using yearly Landsat time series: 2. TimeSync — Tools for calibration and validation - ScienceDirect (Accessed: 28 December 2021).

ELTI, 2012. Training on Coal Mine Site Rehabilitation for Field Practitioners. *ELTI Asia*, Available at: https://elti.yale.edu/sites/default/files/rsource_files/mining_pract_2012.pdf (Accessed: 10 January 2022).

Fornacca, D., Ren, G., Xiao, W., 2018. Evaluating the Best Spectral Indices for the Detection of Burn Scars at Several Post-Fire Dates in a Mountainous Region

of Northwest Yunnan, China. *Remote Sensing*, 10(8), p. 1196. Available at: https://www.mdpi.com/2072-4292/10/8/1196/htm (Accessed: 2 January 2022).

Fuller, D.O., Meijaard, E.M. Christy, L., Jessup, T.C., 2010. Spatial assessment of threats to biodiversity within East Kalimantan, Indonesia. *Applied Geography*, 30(3), pp. 416-420. Available at: https://www.sciencedirect.com/science/article/pii/S014362280900085X?casa_token=Y85VmD2vExMAAAAA:X4uAHH-VY5806aKO9t461pHZDkON4_FKEMFHXVZjWmTpDQfuC-M_DNz9okqdihtJCSOswBg6u-Q (Accessed: 15 January 2022).

Google Earth 6.2, (2022) PT Singlurus Pratama coal mine 1°00'48.6"S 116°55'19.0"E, elevation 100M. [Online] Available at: http://www.google.com/earth/index.html (Accessed: 4 January 2022).

Grădinarua, S.R., Kienasta, F., Psomas, A., 2019. Using multi-seasonal Landsat imagery for rapid identification of abandoned land in areas affected by urban sprawl. Ecological Indicators, 96, pp. 79-86. Available at: file:///C:/Users/1660B~1.UNI/GEOG60~3/ASSIGN~1/ASSESS~1/LITERA~1/Week9/RECOMM~1/2019US~1.PDF (Accessed: 11 January 2022).

Hansen, M. C., P. V. Potapov, R. Moore, M. Hancher, S. A. Turubanova, A. Tyukavina, D. Thau, S. V. Stehman, S. J. Goetz, T. R. Loveland, A. Kommareddy, A. Egorov, L. Chini, C. O. Justice, and J. R. G. Townshend. 2013. “High-Resolution Global Maps of 21st-Century Forest Cover Change.” *Science*, 342, pp. 850–53. Available at: https://developers.google.com/earth-engine/datasets/catalog/UMD_hansen_global_forest_change_2020_v1_8#citations (Accessed: 11 January 2022).

Hereher, M.E., 2015. Environmental monitoring and change assessment of Toshka lakes in southern Egypt using remote sensing. *Environmental Earth Sciences*, 73, pp. 3623–3632. Available at:

https://link.springer.com/article/10.1007/s12665-014-3651-5 (Accessed: 3 January 2022).

Kennedy, R.E., Yang, Z., Cohen, W.B., 2010. Detecting trends in forest disturbance and recovery using yearly Landsat time series: 1. LandTrendr — Temporal segmentation algorithms. *Remote Sensing of Environment*, 114, pp. 2897–2910. Available at: https://www.sciencedirect.com/science/article/pii/S0034425710002245 (Accessed: 16 January 2022).

Kennedy, R.E., Yang, Z., Cohen, W.B., Pfaff, E., Braaten, J. and Nelson, P., 2012. Spatial and temporal patterns of forest disturbance and regrowth within the area of the Northwest Forest Plan. *Remote Sensing of Environment*, 122, pp.117-133.

Kennedy, R.E., Yang, Z., Cohen, W.B., Rfaff, E., Braaten, J., Nelson, P., 2012. Spatial and temporal patterns of forest disturbance and regrowth within the area of the Northwest Forest Plan. *Remote Sensing of Environment*, 122. Pp. 117-133.

Key Engineering Materials, 500, pp. 492–499. Available at: https://www.scientific.net/KEM.500.492 (Accessed: 10 January 2022).
Kraemer, R., Prishchepov, A.V.. Müller, D., Kuemmerle, T., Radeloff, V.C., Dara, A., Terekhov, A., Frühauf, M., 2015. Long-term agricultural land-cover change and potential for cropland expansion in the former Virgin Lands area of Kazakhstan. Environmental Research Letters, Available at: 10. https://iopscience.iop.org/article/10.1088/1748-9326/10/5/054012/meta (Accessed: 9 January 2022).

Li, X., Lanorte, A., Lasaponara, R., Lovallo, M., Song, W., Telesca, L., 2017. Fisher–Shannon and detrended fluctuation analysis of MODIS normalized difference vegetation index (NDVI) time series of fire-affected and fire-

unaffected pixels. *Geomatics, Natural Hazards and Risk*, Available at: https://www.researchgate.net/publication/260700522_Fisher-Shannon_information_plane_analysis_of_SPOTVEGETATION_Normalized_Difference_Vegetation_Index_NDVI_time_series_to_characterize_vegetation_recovery_after_fire_disturbance (Accessed: 28 December 2021).

Schmidt, M., Pringle, M., Devadas, R., Denham, R., Dan, T., 2016. A Framework for Large-Area Mapping of Past and Present Cropping Activity Using Seasonal Landsat Images and Time Series Metrics. *Remote Sensing*, 8(4), p. 312. Available at: https://www.mdpi.com/2072-4292/8/4/312 (Accessed: 2 January 2022).

USGS, 2022. Landsat Satellite Missions. Available at: https://www.usgs.gov/landsat-missions/landsat-satellite-missions (Accessed: 11 January 2022).

Woodbury, D.J. and Arbainsyah, 2020. Being realistic about coal mine rehabilitation in Indonesia: An ecological perspective. *Mongabay Series: Indonesian coal*. Available at: https://news.mongabay.com/2020/12/being-realistic-about-coal-mine-rehabilitation-in-indonesia-an-ecological-perspective/ (Accessed: 10 January 2022).

Woodbury, D.J. Yassir, I., Arbainsyah, Danica A. Doroski, D.A., Queenborough, S.A., Ashton, M.S., 2019. Filling a void: Analysis of early tropical soil and vegetative recovery under leguminous, post-coal mine reforestation plantations in East Kalimantan, Indonesia. *Land Degradation and Development*, 31(1), pp. 473-487. Available at: https://www.researchgate.net/publication/336884411_Filling_a_void_Analysis_of_early_tropical_soil_and_vegetative_recovery_under_leguminous_post-coal_mine_reforestation_plantations_in_East_Kalimantan_Indonesia (Accessed: 8 January 2022).

Woodcock, C.E., Richard, A., Martha, A., Alan, B., Robert, B., Warren, C., Feng, G., Goward, S.N., Dennis, H., Eileen, H., 2008. Free access to Landsat imagery. *Science*, 320, p. 1011. Available at: https://www.fs.fed.us/global/iitf/pubs/ja_iitf_2008_woodcock001.pdf (Accessed: 6 January 2022).

Yina, H., Pflugmacher, D., Li, A., Li, Z., Hostert, P., 2018. Land use and land cover change in Inner Mongolia – understanding the effects of China's re-vegetation programs. *Remote Sensing of Environment*, 204, pp. 918-930. Available at: 2018. Land use and land cover change in Inner Mongolia - understanding the effects of China's re-vegetation programs.pdf (Accessed: 10 January 2022).

Zhang, P.L., Bo, L.R., Chao, J., 2012. An Object-based Basic Farmland Change Detection Using High Spatial Resolution Image and GIS Data of Land Use Planning.

Zhu, L., Liu, X., Wu, L., Tang, Y. and Meng, Y., 2019. Long-Term Monitoring of Cropland Change near Dongting Lake, China, Using the LandTrendr Algorithm with Landsat Imagery. *Remote Sensing*, 11(10), p.1234.

Zhu, L., Liu, X., Wu, L., Tang, Y., Meng, Y., 2019. Long-Term Monitoring of Cropland Change near Dongting Lake, China, Using the LandTrendr Algorithm with Landsat Imagery. *Remote Sensing*, 11(10), p. 1234. Available at: https://www.mdpi.com/2072-4292/11/10/1234 (Accessed: 4 January 2022).

Sheoran, V., Sheoran, A.S., Poonia, P., 2010. Soil Reclamation of Abandoned Mine Land by

Revegetation: A Review. *International Journal of Soil, Sediment and Water*, 3(2), pp. 2-10. Available at: https://scholarworks.umass.edu/intljssw/vol3/iss2/13/ (Accessed: 10 January 2022).

Xu, H., Wei, Y., Liu, C., Li, X. and Fang, H., 2019. A Scheme for the Long-Term Monitoring of Impervious− Relevant Land Disturbances Using High

Frequency Landsat Archives and the Google Earth Engine. *Remote Sensing*, 11(16), p.1891.

Kennedy, R.E., Yang, Z., Gorelick, N., Braaten, J., Cavalcante, L., Cohen, W.B., Healey, S., 2018. Implementation of the LandTrendr Algorithm on Google Earth Engine. *Remote Sensing*, 10(5), p. 691. Available at: https://www.mdpi.com/2072-4292/10/5/691/htm (Accessed: 11 January 2022).

Sheoran, V., Sheoran, A.S., Poonia, P., 2010. Soil Reclamation of Abandoned Mine Land by Revegetation: A Review. International Journal of Soil, Sediment and Water, 3(2), pp. 2-10. Available at: https://scholarworks.umass.edu/intljssw/vol3/iss2/13/ (Accessed: 11 January 2022).

Muslim, T., 2017. Herpetofauna community establishment on the micro habitat as a result of land mines fragmentation in East Kalimantan, Indonesia. Biodiversitas Journal of Biological Diversity, 18(2), pp. 709-714. Available at: https://www.researchgate.net/publication/316927192_Herpetofauna_community_establishment_on_the_micro_habitat_as_a_result_of_land_mines_fragmentation_in_east_Kalimantan_Indonesia (Accessed: 5 January 2022).

Links to the Google Earth Engine code

Link 1 Hansen global forest:

https://code.earthengine.google.com/?scriptPath=users%2Fostapoutao%2FRemote_Sensing_Practical1%3ACoalMine_2

Link 2 Forest recovery:

https://code.earthengine.google.com/?scriptPath=users%2Fostapoutao%2FRemote_Sensing_Practical1%3ACoalMine_gain

Link 3 Forest disturbance:

https://code.earthengine.google.com/?scriptPath=users%2Fostapoutao%2FRemote_Sensing_Practical1%3ACoalMine_loss

Link 4 Pixel Time Series for the site:

https://code.earthengine.google.com/?scriptPath=users%2Fostapoutao%2FRemote_Sensing_Practical1%3ACoalMine_8_PixelZone